Journal of Catalysis 270 (2010) 163–171

Contents lists available at ScienceDirect

Journal of Catalysis

journal homepage: www.elsevier.com/locate/jcat

An experimental and theoretical investigation of the structure and reactivity of bilayered $VO_x/TiO_x/SiO_2$ catalysts for methanol oxidation

William C. Vining, Anthony Goodrow, Jennifer Strunk, Alexis T. Bell *

University of California, Berkeley, Department of Chemical Engineering, Berkeley, CA 94720-1462, United States

ARTICLE INFO

Article history:
Received 13 August 2009
Revised 6 November 2009
Accepted 22 December 2009
Available online 2 February 2010

Keywords:
Vanadia
Silica
Titania
Methanol oxidation
Kinetics
Theoretical analysis

ABSTRACT

This study reports the results of a combined experimental and theoretical investigation of a bilayered $VO_x/TiO_x/SiO_2$ catalyst consisting of vanadia deposited onto silica containing a submonolayer of titania. Raman spectroscopy indicates that Ti atoms are bonded to the silica support via Ti—O—Si bonds, and Raman and EXAFS data indicate that the vandia is present as isolated vanadate groups bonded to the support through V—O—Si and V—O—Ti bonds. For a fixed vanadia surface density (0.7 V/nm^2), the turnover frequency for methanol oxidation to formaldehyde increases with increasing Ti surface density (0.2–2.8 Ti/nm^2) and the apparent activation energy decreases. These trends are well represented by a model of the active site and its association with Si and Ti atoms of the support. This model takes into account the distribution of Ti on the silica support, the fraction of active sites with 0, 2, and 3 V—O—Ti support bonds, and the rate parameters determined for each of these active sites determined from quantum chemical calculations and absolute rate theory.

1. Introduction

The selective oxidation of methanol to formaldehyde has been shown to be catalyzed by isolated vanadate groups supported on metal oxides, such as SiO_2, Al_2O_3, TiO_2, ZrO_2, and CeO_2 [1–8]. The structure of the active center has been deduced from evidence obtained by EXAFS and Raman spectroscopy; it consists of a central V atom bonded to the support through 3 V—O—M bonds (M = Si, Al, Ti, Zr, Ce) and a single V=O vanadyl bond [7,8]. The activity of these sites strongly depends on support composition [1,2,5,7,8]. For example, the turnover frequency (TOF) for methanol oxidation on VO_x/TiO_2 is roughly 10^3 higher than that for VO_x/SiO_2 at the same reaction conditions. Previous studies have concluded that the activity of the vanadate sites increases with decreasing Sanderson electronegativity of the support metal cation [2,5,9]. While this interpretation leads to a good correlation of catalyst activity with Sanderson electronegativity, it is not supported by compelling theoretical arguments. For instance, if the Sanderson electronegativity of the support metal cation was the sole reason for the increased activity, then the thermodynamics of the adsorption step would vary greatly because it is the only step involving the metal support atom. Since the adsorption energy of methanol on different metal oxide supports is comparable [5], a large variation in entropy must then exist, which is unlikely for the same reaction. By contrast, a recent theoretical study aimed at understanding the higher activity of VO_x/TiO_2 relative to VO_x/SiO_2 has shown that O-vacancies in TiO_2 can increase the reaction rate by lowering the activation energy of the rate-determining step [10]. Submonolayer quantities of titania dispersed on silica have also been found to increase the activity of dispersed vanadia by over an order of magnitude [11–14]. The aim of the present work was to develop a deeper understanding of the origins of the enhanced activity of isolated vanadate species supported on silica containing submonolayer quantities of titania. To this end, theoretical and experimental studies were carried out to understand the role of Ti atoms on bilayered $VO_x/TiO_x/SiO_2$ catalyst. Samples were characterized by X-ray absorption near-edge spectroscopy (XANES), extended X-ray absorption fine structure (EXAFS), and Raman spectroscopy. The rate parameters involved in the oxidation of methanol were determined using density functional theory (DFT) and absolute rate theory.

2. Experimental methods

A mesoporous silica support with high surface area, MCM-48, was prepared as described previously [7]. The BET surface area was measured by N_2 physisorption with an Autosorb-1 instrument. Prior to N_2 adsorption/desorption measurements, each sample was treated under vacuum for 12 h at 393 K. The single-point BET method was used to determine the surface area, and the total pore volume was calculated from the desorption isotherm using the method of Barrett, Joyner, and Halenda (BJH). The concentration of silanols on the MCM-48 support was determined by reacting

* Corresponding author. Fax: +1 510 642 4778.
E-mail address: alexbell@berkeley.edu (A.T. Bell).

0021-9517/$ - see front matter © 2009 Elsevier Inc. All rights reserved.
doi:10.1016/j.jcat.2009.12.017

$Mg(CH_2Ph)_2{\cdot}2THF$ with the Brønsted acid sites and monitoring the evolved toluene by ^1H NMR using a known quantity of ferrocene as an internal standard [15].

Prior to each metal grafting step, the MCM-48 support was heated to 393 K under dynamic vacuum (<27 Pa) to remove any physisorbed water. Titanium was grafted under a N_2 atmosphere onto the MCM-48 via impregnation with a solution of $Ti(O^iPr)_4$ dissolved in approximately 60 cm^3 of anhydrous toluene. The mixture was stirred for 4 h at ambient temperature and then rinsed 2–3 times with ~60 cm^3 anhydrous toluene per rinse before drying under vacuum. The as-prepared catalyst was then transferred to a furnace under inert atmosphere, where it was treated in He flowing at a rate of 50 cm^3/(min g-catalyst) and heated at 2 K/min from 298 to 573 K. Dry air flowing at 50 cm^3/(min g-catalyst) was then passed over the sample as the temperature was ramped at 2 K/min from 573 to 773 K, where it was held for 4 h. Subsequent Ti grafting steps were performed in the same manner to increase the surface coverage of Ti. Vanadium was grafted onto the previously prepared TiO_x/SiO_2 sample via impregnation with a solution of $O{=}V(O^iPr)_3$ in 60 cm^3 anhydrous toluene in a manner analogous to that used to graft Ti onto the support.

Catalyst metal weight loadings were determined by inductively coupled plasma (ICP) at Galbraith Labs. The surface densities of Ti and V were calculated based upon the surface area of the catalyst determined by N_2 physisorption after metal grafting.

Raman spectra were recorded with a 532 nm frequency-doubled Nb:YAG laser using a 25 mW power measured at the sample. The catalyst was pressed into a 20 mg pellet at 28 MPa and was then pretreated in flowing air at 60 cm^3/min from 298 to 773 K. Heating at 773 K was continued for at least 1 h to reduce the fluorescence background. Samples were mounted onto a holder and were rotated at 150 Hz in a quartz Raman cell to prevent sample damage by the laser. Spectra were recorded at a resolution of 2 cm^{-1} with a collection time of 2 s at room temperature after pretreatment.

X-ray absorption spectroscopy (XAS) measurements were performed at the Stanford Synchrotron Radiation Laboratory (SSRL) on beam lines 2–3 and 10–2 using a Si(1 1 1) crystal. Data were acquired at the V and Ti K-edges, and the energy was calibrated using a metal foil placed between two ionization chambers located after the sample. The metal edge was calibrated to the first inflection point of the main peak for V and Ti and set to 5465 and 4966 eV, respectively. Sample weights were calculated to obtain an absorbance of ~2.5 in order to obtain the optimal signal to noise ratio [16], and boron nitride was added to make a self-supporting pellet. Samples were placed in a controlled-atmosphere cell that could be heated up to 823 K in the presence of flowing gas [17]. The cell was evacuated to 6×10^{-4} Pa at ambient temperature and cooled to 84 K before collecting the XAS data. XANES measurements were taken under flowing gases at reaction temperature.

The XAS data were analyzed with the software IFEFFIT and its complementary GUIs Athena and Artemis [18,19]. The edge energy of the sample was defined as the first inflection point after the pre-edge feature. The data were normalized by subtracting a pre-edge line fit to the data from −150 to −30 eV relative to the edge energy, then a quadratic polynomial was fit with a k-weight of 2 to the data from 150 to 950 eV for EXAFS and 100–300 eV for XANES, both relative to the edge energy. A cubic spline was then fit to the data from 0 to 15.6 $Å^{-1}$ with background frequencies below 0.9 Å minimized and subtracted from the data to obtain the EXAFS signal. Finally, the EXAFS data were Fourier transformed with a Hanning window over a range from 2 to 11 Å to optimize the signal to noise ratio. The oxidized samples were fit with k-weights of 1, 2, and 3 in the range $0.9 < R < 3.4$ Å.

Temperature-programmed reaction (TPR_x) measurements were performed after treating the catalyst to 773 K under UHP 20% O_2/balance He for 1 h. Ultra high purity (UHP) He and O_2 were flowed through a methanol saturator held at a constant temperature of 273 K to maintain a reactant mixture of 0.04:0.07:0.89 MeOH:O_2:He at a total pressure of 101 kPa. The temperature was ramped from 373 to 773 K at 2 K/min, and the composition of the effluent gas was monitored with a Cirrus quadrupole mass spectrometer. The intensities of the peaks recorded for each product were normalized using He (mass 4) as the internal standard. Species concentrations were obtained by inverting the raw data using matrix deconvolution and a calibration matrix.

3. Theoretical methods

Density functional theory (DFT) was used to determine optimized geometries, vibrational frequencies, and thermodynamic properties for all species. All DFT calculations were performed within QChem 3.0 [20]. The B3LYP functional and 6-31G* basis sets were used for all atoms, except for Ti and V, which were treated using an effective core potential and LANL2DZ basis sets. All atoms were allowed to relax during geometry optimization calculations. The calculated vibrational frequencies were scaled by 0.9614 to account for the overestimation predicted at the B3LYP/6-31G* level of theory [21].

The growing string method (GSM) [22,23] was used to determine an initial guess of the transition state geometry. The transition state estimate was then refined by performing a transition state search using the eigenvector following (EF) algorithm in QChem 3.0. Each transition state search consisted of three parts: (1) an initial analytical Hessian calculation, (2) a transition state optimization, and finally (3) a frequency calculation to verify the presence of one imaginary frequency corresponding to the motion of atom(s) associated with the transition state. The broken symmetry approach [24,25] was used to calculate the activation energy for reactions involving a biradicaloid electronic structure with multiple spin states, as described in previous work [10,26,27]. The Landau–Zener probabilities for spin-surface crossing reactions [28–30] were calculated as done previously [31]. The rate constant for spin-surface crossing was ~10^6–10^7 times greater than the rate constant for the rate-limiting step at 550 K for all cases. To obtain more accurate estimates of the reaction and activation energies, single-point calculations were performed on all optimized reactant, product, and transition state geometries. All basis sets were augmented to include diffuse and polarization functions; for instance, all non-metal atoms were treated using the 6-311++G** basis sets.

The Gibbs free energy for all structures was calculated using the standard equations from statistical mechanics [32,33]. The translational, rotational, and vibrational partition functions were computed explicitly, as done in previous work [10,27]. The standard state for all Gibbs free energies reported in this work was 550 K and has been denoted as $\Delta G°$. The standard state used for gas-phase species was taken to be 1 atm, and a mole fraction of 1 was used for all vanadia species.

4. Results

4.1. Catalyst characterization

The single-point BET surface area ranged from 1522 to 1567 m^2/g for MCM-48 before grafting. These surface area measurements are consistent with values reported in the literature for samples up to 1600 m^2/g [34,35]. Total pore volumes of the silica support ranged from 0.84 to 0.87 cm^3/g, consistent with previously reported values [7]. The concentration of silanols on the support was 1.69 OH/nm^2, which is similar to values reported for silica

Table 1
BET surface area, pore volume, and metal surface coverages for each catalyst.

Catalyst	Surface Area (m^2/g)	Avg. pore size (Å)	Vanadium loading (V/nm^2)	Titanium loading (Ti/nm^2)
0.3 VO_x/SiO_2	1335	21	0.3	–
0.6 VO_x/0.2 TiO_x/SiO_2	1201	20	0.6	0.2
0.7 VO_x/0.9 TiO_x/SiO_2	1045	19	0.7	0.9
0.7 VO_x/1.4 TiO_x/SiO_2	1059	18	0.7	1.4
0.7 VO_x/2.8 TiO_x/SiO_2	923	20	0.7	2.8

heated to 723 K [36]. The surface area decreased to ~1000 m^2/g after grafting V and Ti, for all but the lowest Ti weight loading, as shown in Table 1. Similar values for the surface area have been reported previously [34].

The metal weight loadings for all catalysts are shown in Table 1. Five catalysts with varying Ti coverages were synthesized, including a reference sample without Ti. The vanadium surface coverage for each sample was held constant at 0.7 V/nm^2 to ensure isolated vanadate sites [7], except in the sample without Ti present, as trace amounts of V_2O_5 were detected on VO_x/SiO_2 from Raman spectroscopy at that coverage.

The Raman spectra in Fig. 1 of the MCM-48 support show broad peaks centered at 607 and 458 cm^{-1} indicative of the D_1 and D_2 bands of silica, respectively [36]. The spectra of the TiO_x/SiO_2 supports show additional peaks at 918 and 1080 cm^{-1}, indicative of Si—O—Ti vibrations [37,38]. Peaks were not observed at 146, 197, 397, 516, 640, 800 cm^{-1} or 143, 447, 612, 826 cm^{-1}, characteristic of anatase [8] or rutile [35], respectively. For this reason, it is concluded that all of the Ti is atomically dispersed on the surface of MCM-48.

As seen in Fig. 1, the Raman spectra taken after grafting vanadium onto the support shows a vanadyl band at 1037–1039 cm^{-1}. The frequency of this band is consistent with what has been reported for vanadium supported on SiO_2 [7] and TiO_x/SiO_2 [39] and matches the vanadyl frequency shown for 0.3 VO_x/SiO_2. Broad bands at 500–800 cm^{-1} and 200–300 cm^{-1} corresponding to V—O—V vibrations were not observed nor were bands at 998, 702, 529, or 287 cm^{-1}, characteristic of V_2O_5 [40]. No evidence of crystalline TiO_x was seen upon V grafting, indicating the absence of anatase or rutile in the sample. The peak at 607 cm^{-1} is attributed to 3-ring siloxane bridges and shifts towards a broad peak centered at 659 cm^{-1} upon V grafting, which could indicate V—O—Ti bonds [41].

EXAFS and XANES data were acquired at both the V and Ti K-edges. Examination of the edge energy of Ti in each sample indicates that it is predominantly in the 4+ oxidation state. Farges et al. [42] have shown that the height and energy of the pre-edge feature can indicate the coordination of Ti^{4+} species. Fig. 2 shows that the pre-edge energy of 4979.7 eV is consistent with 4-coordinated Ti [42], but the height of the pre-edge feature for 0.9 TiO_x/SiO_2 and 1.4 TiO_x/SiO_2 is lower than that found typically for a fully allowed transition. A reference scan of anatase was used to align the energy with the data of Farges et al. [42]. These authors propose that a smaller than expected pre-edge peak could be indicative of a mixture of 4- and 5-coordinated or 4- and 6-coordinated Ti. A lower pre-edge height, however, can also be attributed to a distorted tetrahedral geometry from HO—Ti(OSi—)$_3$ that one would expect to see upon grafting and activation on the surface of the silica support [43], as a consequence of lower 3d–4p Ti orbital hybridization and less overlap with the 2p O orbitals than could be observed for the purely tetrahedral case. Most likely, both factors contribute to the reduction in the pre-edge peak, with coordination effects resulting in a lower peak for 1.4 TiO_x/SiO_2 than 0.9 TiO_x/SiO_2.

After grafting V onto the 0.9 TiO_x/SiO_2 samples, the Ti K-edge energy did not change but the pre-edge feature decreased from 0.49 to 0.26, indicating an interaction between V and Ti after grafting and activation. Interestingly, the pre-edge feature decreased in the higher Ti loading sample to 0.37, but the decrease was less than that for the 0.9 TiO_x/SiO_2 sample. This result is expected, since for a given quantity of V—O—Ti interactions, the 1.4 Ti sample would have a smaller fraction of Ti interacting with V than the 0.9 Ti sample, and hence, the average effect on the XANES would be less pronounced. Therefore, the smaller decrease in pre-edge intensity for 0.7 VO_x/1.4 TiO_x/SiO_2 relative to 0.7 VO_x/0.9 TiO_x/SiO_2 is most likely a result of a smaller fraction of the Ti interacting with V.

Examination of the V K-edge indicates that most of the vanadium is in the 5+ oxidation state, since the edge energy, 5484.34 eV, is consistent with the edge energies of both V_2O_5 and $NaVO_3$, 5484.58 eV and 5482.78 eV, respectively, as shown in Fig. 3. In addition, the height of the pre-edge feature, which reflects the hybridization of the metal 3d and 4p orbitals, is consistent with a 5+ oxidation state. The V K-edge XANES for the other $VO_x/TiO_x/SiO_2$ samples and 0.3 VO_x/SiO_2 are the same as for 0.7 VO_x/0.9 TiO_x/SiO_2 and are not shown.

The fit of the V K-edge EXAFS data for 0.7 VO_x/0.9 TiO_x/SiO_2, shown in Fig. 4 indicates that there are two oxygen shells at 1.58 ± 0.01 Å and 1.77 ± 0.01 Å. The shorter V—O bond distance is

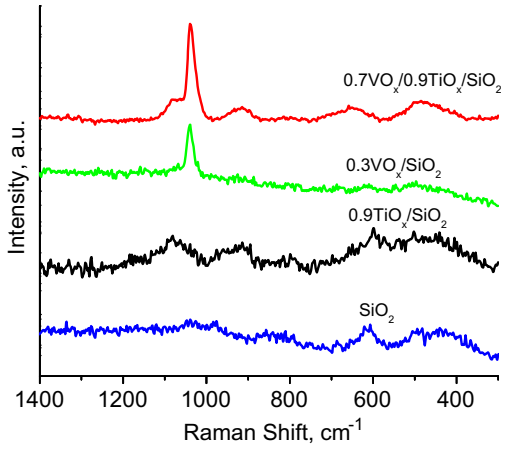

Fig. 1. Raman spectra for SiO_2, 0.9 TiO_x/SiO_2, 0.3 VO_x/SiO_2, and 0.7 VO_x/0.9 TiO_x/SiO_2. Samples were pretreated in 20% O_2/balance He at 773 K. Scans were taken at ambient temperature in UHP He following pretreatment.

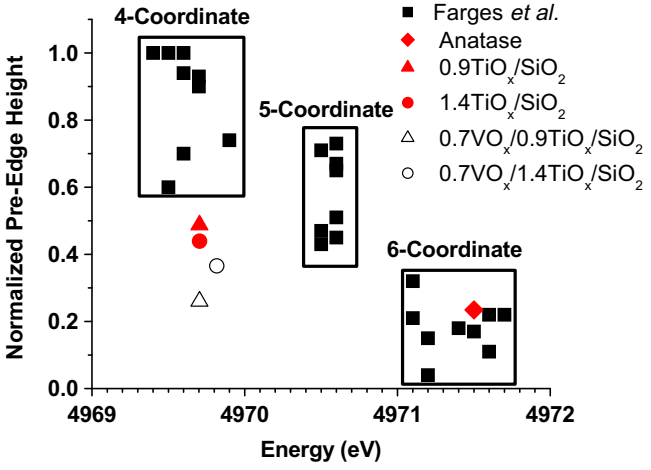

Fig. 2. Pre-edge peak heights obtained from Ti K-edge normalized XANES for x TiO_x/SiO_2 and y VO_x/x TiO_x/SiO_2. Samples were pretreated in 20% O_2/balance He at 773 K. Scans were taken at LN2 temperature under vacuum.

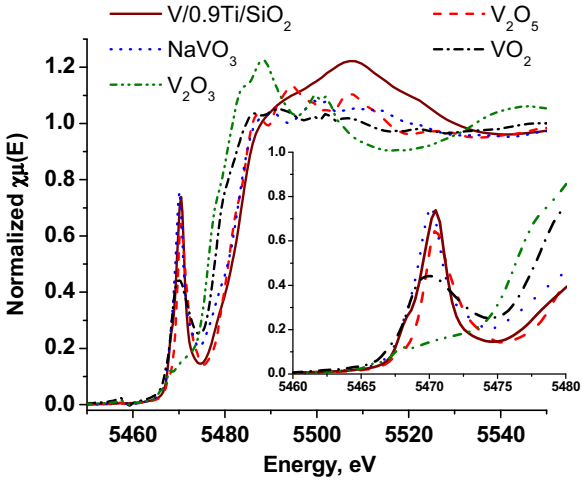

Fig. 3. V K-edge XANES data for $0.7VO_x/0.9TiO_x/SiO_2$ (——) after pretreatment at 773 K in UHP 20% O_2/balance He, $NaVO_3$ (- - - -), V_2O_5 (— — —), VO_2 (—·—·—), and V_2O_3 (—·· —·· —). Scans taken at room temperature. The inset shows a close-up of the pre-edge feature. XANES data for the other catalysts are similar and not shown for clarity.

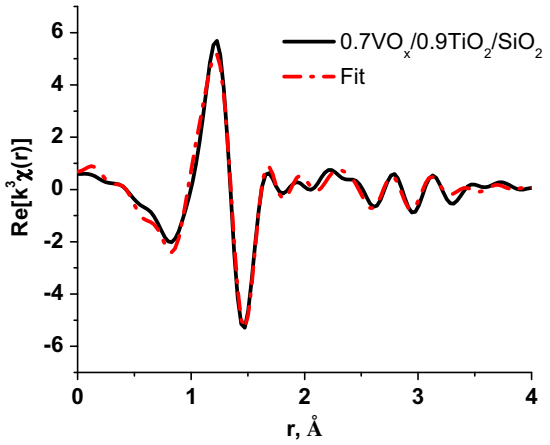

Fig. 4. Real space Fourier transformed k^3-weighted $\chi(k)$ for 0.7 VO_x/0.9 TiO_x/SiO_2 treated in synthetic air up to 773 K and the corresponding fit to the data. Scans were taken at 84 K and $<6 \times 10^{-4}$ Pa. The data were fit over the range from 0.9 to 3.4 Å for k-weights of 1, 2, and 3.

consistent with a vanadyl oxygen, while the longer bond is indicative of a V—O single bond [7] possibly connected to a Si or Ti atom. A Si shell was fit with a V—Si distance of 3.32 ± 0.19 Å from the absorbing vanadium. A backscattering Ti atom was fit to the data at a distance of 3.34 ± 0.05 Å, which could be indicative of either a V or Ti backscattering atom because of the closeness in the atomic numbers of the two atoms, but is more likely attributable to Ti because of the appearance of a Raman peak at 659 cm^{-1}, characteristic of V—O—Ti vibrations [40], and the reduction in Ti pre-edge intensity in the Ti XANES. These measurements are summarized in Table 2, and more details of the fit can be found in the Supplementary material for this catalyst. The bond distances obtained from fitting the EXAFS data for the other $VO_x/TiO_2/SiO_2$ samples were similar to those obtained for the 0.7 VO_x/0.9 TiO_x/SiO_2 sample.

4.2. Catalysis

The results of TPR_x studies for each of the $VO_x/TiO_x/SiO_2$ catalysts are qualitatively similar. The TPR_x results from the 0.9 Ti grafted sample are shown as a representative case in Fig. 5. For each catalyst sample, CH_2O and H_2O are formed in a 1:1 ratio at the onset of methanol oxidation. As the temperature rises, CH_2O decomposes to form CO and H_2, which rapidly reacts to form water, and a small fraction of the CO undergoes oxidation to CO_2. The primary difference between VO_x/SiO_2 and the samples of $VO_x/TiO_x/SiO_2$ is the temperature at which CH_2O first appears. The peak temperature shifts from 700 K for VO_x/SiO_2 to 573 K for all samples except the lowest Ti weight loading, even though the production of formaldehyde begins at the same temperature for all samples with Ti.

Table 2
Comparison between theoretical and experimental measurements of the active site. The theoretical values are similar for each of the active sites shown in Fig. 7. The experimental values for bond lengths are obtained from the EXAFS fit in Fig. 4, and the vibrational frequencies are from Raman spectroscopy.

	Theory	Experiment
r(V=O)	1.57 Å, 1.58 Å	1.58 ± 0.01 Å[a]
r(V—O)	1.76 Å, 1.77 Å	1.77 ± 0.01 Å[a]
r(V—Si)	3.28 Å	3.32 ± 0.19 Å[a]
r(V—Ti)	3.40 Å	3.34 ± 0.05 Å[a,b]
ν(V=O)	1030 cm^{-1}, 1033 cm^{-1}	1037–1039 cm^{-1}[1a]
ν(Si—O—Ti)	924 cm^{-1}, 1073 cm^{-1}	918 cm^{-1}[1a,c], 1080 cm^{-1}[1a,c]

[a] Present work.
[b] Cannot discern between V—Ti and V—V backscattering but assumed to correspond to V—Ti bond length from Ti XANES and Raman.
[c] Ref. [39].

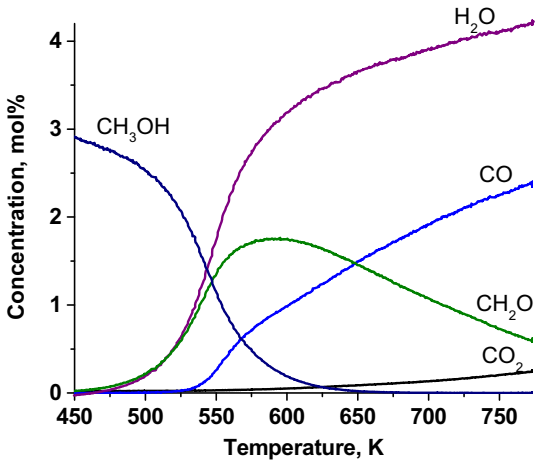

Fig. 5. TPR_x data for methanol oxidation on $0.7VO_x/0.9\ TiO_x/SiO_2$. The temperature was ramped at 2 K/min in a mixture of 0.04 MeOH/0.07 O_2/balance He.

Fig. 6 shows an Arrhenius plot with the apparent activation energy for each catalyst. These results may then be compared to those reported by Bronkema et al. on silica- and titania-supported vanadium [7,8]. The apparent activation energy measured for the $VO_x/TiO_x/SiO_2$ samples ranges from 21 kcal/mol (for the 0.7 VO_x/0.2 TiO_x/SiO_2 sample) to 18 kcal/mol (for the 0.7 VO_x/2.8 TiO_x/SiO_2 sample). These values fall between those for VO_x/SiO_2 (23 kcal/mol) and VO_x/TiO_2 (16 kcal/mol), demonstrating that the activation energy of the reaction decreases as the loading of Ti increases.

4.3. Theoretical representation of $VO_x/TiO_x/SiO_2$

Based on the experimental results indicating the presence of isolated V sites, the titania–silica support was represented by a model similar to that used to represent isolated vanadate sites

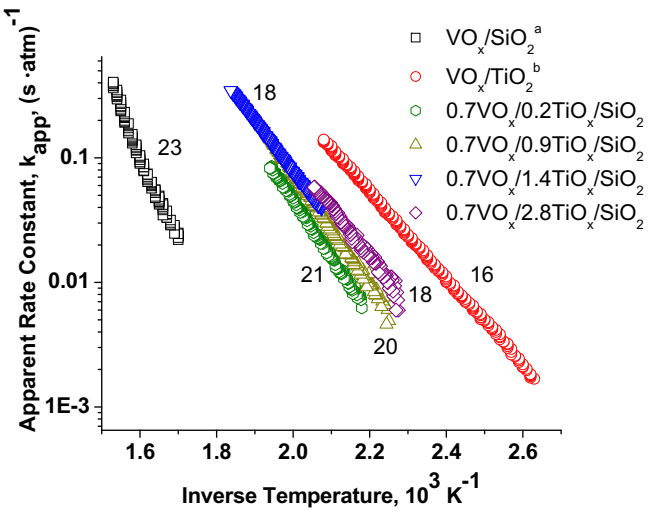

Fig. 6. Arrhenius plot and apparent activation energies in kcal/mol for 0.7 VO_x/y TiO_2/SiO_2 obtained from TPR_x experiments carried out with 0.04 MeOH/0.07 O_2/balance He with a temperature ramp of 2 K/min ([a]Ref. [7] SiO_2. [b]Ref. [8] TiO_2).

on silica [26,27] and titania [10], as shown in Fig. 7. In this model, the support is represented as a silsesquioxane structure (cubic $Si_8O_{12}H_8$ with terminating H atoms), containing either all Si or Ti atoms. The silsesquioxane model was found in previous work [27] to provide a very good estimate of experimentally measured bond lengths, bond angles, D_1 and D_2 breathing modes, and coordination environment of Si. The vanadate species is then introduced by removing one of the corner Si or Ti atoms and replacing it with a V=O unit. The optimized geometries of such cluster representations of VO_x/SiO_2 and VO_x/TiO_2 were shown to agree closely with experimental measurements and yielded estimates of the reaction energetics and the rate parameters for methanol oxidation that corresponded closely to those measured experimentally [10,27]. Although these DFT calculations considered 4-coordinated Ti cluster models, the geometry, vibrational frequencies, and adsorption energies for small molecules were shown to be in good agreement with more extensive slab calculations and with experimental values, where surface Ti atoms are generally 5-coordinated [10].

The cluster model used previously to describe VO_x/SiO_2 was modified by systematically increasing the number of Ti atoms by replacing Si atoms in order to increase the number of V—O—Ti support bonds from zero to three. Active sites with and without an O-vacancy were considered for species with 1 or more V—O—Ti support bonds. O-vacancies have been shown to play a role in the enhanced activity of VO_x/TiO_2 [10] and have recently been observed on TiO_x/SiO_2 samples identical to those used for this study (see Supplementary material). All sites comprised of 3 V—O—Si support bonds were assumed to be free of O-vacancies because formation of an O-vacancy from a Si—O—Si bond in silica is energetically much less favorable than from a Ti—O—Si bond or a Ti—O—Ti bond in titania. For instance, the defect formation energy on SiO_2 is 196 kcal/mol (8.5 eV), [44] compared to 98 kcal/mol (4.27 eV) on the anatase phase of TiO_2 [45] and 46 kcal/mol (1.98 eV) on V_2O_5 [45]. O-vacancies next to isolated V atoms are excluded because DFT calculations introducing such a vacancy result in the rearrangement and loss of the vanadyl oxygen in the active site, thereby forming a V^{3+} species. Likewise, since the energy to form a vacancy at a Si—O—Ti bond is higher than that for the formation of a vacancy at a Ti—O—Ti bond, only vacancy formation involving the latter type of bond was considered. The seven different optimized active site geometries are shown in Fig. 7 and are denoted by the number of V—O—Ti support bonds (zero to three) and the presence or absence of an O-vacancy (represented by *d*) as species **0**, **1**, **1d**, **2**, **2d**, **3**, and **3d**. The replacement of terminal H atoms with terminal —OH groups resulted in no change in the optimized geometries or reaction energies for the active sites.

The geometries and frequencies of the seven active sites are in good agreement with the EXAFS and Raman measurements observed experimentally, as seen in Table 2. Where multiple bond lengths or vibrational frequencies are listed, these correspond to the lower and upper values for all active sites shown in Fig. 7. A single theoretical value is listed when the bond length or vibrational frequency is identical for all seven species. The theoretical and experimental V=O and V—O bond lengths are in good agreement and differ by less than 0.2 Å; indeed, the calculated V—Si and V—Ti lengths differ by no more than 0.06 Å from experimental values. The differences between the cubic cluster model of the active site and the structure of the actual catalyst site may be the cause of the small elongation in the V—Si and V—Ti distances. Lastly, the calculated V=O stretch and the symmetric and asymmetric Si—O—Ti stretches agree well with experimental results. The calculated V=O, V—O—Si, and V—O—Ti stretching frequencies do not change significantly as the number of V—O—Ti support bonds is increased. The good agreement between theory and experiment in Table 2 suggests that the species shown in Fig. 7 should provide a reasonable representation of the active sites on the bilayered support.

4.4. Theoretical modeling of methanol oxidation kinetics

Methanol adsorption on the active sites shown in Fig. 7 can be achieved by cleaving a V—O—Si or V—O—Ti support bond to form a

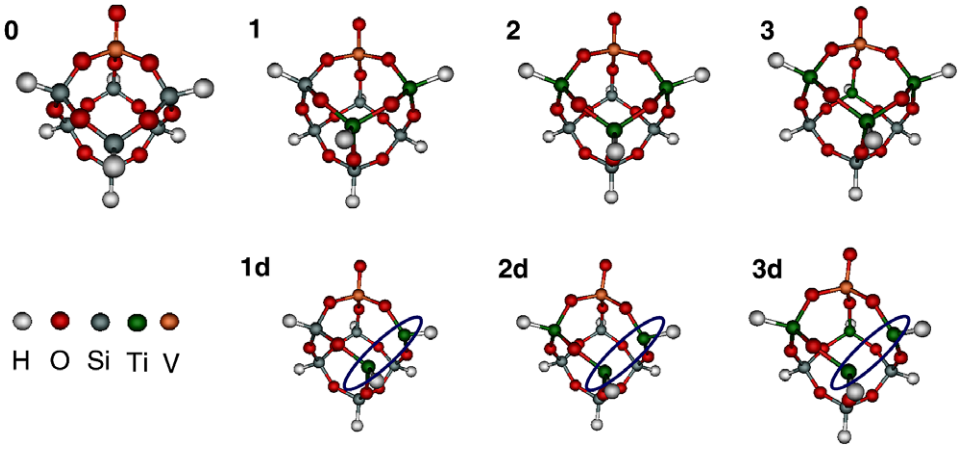

Fig. 7. Active sites with 0, 1, 2, and 3 V—O—Ti support bonds. The species **1d**, **2d**, and **3d** in the second row contain an O-vacancy.

V—OCH_3 species and a Si—OH or Ti—OH species. Previous theoretical calculations have shown that while formation of a V—OH species and a Si—OCH_3 or Ti—OCH_3 species are possible, they are not preferred energetically [10,27]. Experimental work has also shown that V—OCH_3 species are precursors for the formation of formaldehyde [1,5–8].

The adsorption energy for methanol, ΔE_{ads}, was calculated for each of the seven active sites and is shown in Table 3. Cleavage of both the V—O—Si and V—O—Ti support bonds was considered for all cases. ΔE_{ads} was found to be insensitive to the number of V—O—Ti support bonds and to sites with and without an O-vacancy, ranging from −15.5 kcal/mol for an all SiO_2 support (species **0**) to −15.4 kcal/mol for species containing 3 V—O—Ti support bonds (species **3** and **3d**). The small range of calculated values of ΔE_{ads} suggests that the support has little intrinsic electronic effect during methanol adsorption.

For all sites that do not contain an O-vacancy and have at least 1 V—O—Si support bond (species **0**, **1**, and **2**), the V—O—Si bond is the preferred bond to break upon methanol adsorption. However, the reverse is observed for sites that contain an O-vacancy and at least 1 V—O—Si support bond (**1d**, **2d**), in which case the V—O—Ti bond is broken preferentially by 1.0–1.5 kcal/mol. Despite the small difference in MeOH adsorption energy across either the V—O—Ti or V—O—Si bonds, the overall rate for methanol oxidation on sites containing an O-vacancy is one to two orders of magnitude higher than on sites not containing an O-vacancy.

The rate-limiting step in methanol oxidation involves abstraction of one of the three methoxy H atoms to the vanadyl O atom. The broken symmetry approach was used to calculate the activation energy for this step (ΔE_{rls}) because the oxidation state of V changes from V^{5+} with zero *d* electrons in the reactant to V^{3+} with two unpaired *d* electrons in the product [26]. The activation energies for each of the active sites in Fig. 7 are shown in Table 3. For sites without an O-vacancy, ΔE_{rls} decreases slightly with increasing number of V—O—Ti support bonds – from 39.8 kcal/mol for species **0** to 38.6 kcal/mol for species **3**. For sites with an O-vacancy, $\Delta E^{\ddagger}_{rls}$ decreases with increasing number of V—O—Ti support bonds more dramatically – from 38.6 kcal/mol for species **1d** to 34.3 kcal/mol for species **3d**. The reason for the large decrease in $\Delta E^{\ddagger}_{rls}$ for sites with an O-vacancy is the increased flexibility of the support and the strong H-bond stabilization in the transition state.

The apparent activation energy ($\Delta E^{\ddagger}_{app}$) and apparent rate constant at 550 K (k_{app}) are defined by Eqs. (1) and (2), respectively [10,26,27]. The equilibrium constant for methanol adsorption, K_{ads}, is calculated using Eq. (3). The rate constant for the rate-limiting H-abstraction step, k_{rls}, is determined using Eq. (4).

$$\Delta E^{\ddagger}_{app} = \Delta E_{ads} + \Delta E^{\ddagger}_{rls} \tag{1}$$

$$k_{app} = K_{ads} k_{rls} \tag{2}$$

$$K_{ads} = \sigma_{ads} \frac{q_{MeOH\cdot S}}{q_{MeOH} q_S} \exp\left(\frac{PV}{RT}\right) \exp\left(\frac{-\Delta E_{ads}}{RT}\right) \tag{3}$$

$$k_{rls} = \sigma_{rls} \kappa(T) \frac{k_B T}{h} \frac{q^{\ddagger}_{CH_2O\cdot S}}{q_{MeOH\cdot S}} \exp\left(\frac{-\Delta E^{\ddagger}_{rls}}{RT}\right) \tag{4}$$

In Eq. (3), σ_{ads} is the symmetry factor, which is equal to the number of equivalent V—O—M bonds that can be broken during the adsorption of methanol. The partition functions q_{MeOH}, q_S, and $q_{MeOH\cdot S}$ are for methanol, the active site, and the active site with adsorbed methanol, respectively. In Eq. (4), σ_{rls} is the symmetry factor for the rate-limiting step and is equal to three, because of the three equivalent methoxy H atoms that can be abstracted. The transmission coefficient for tunneling, $\kappa(T)$, is calculated using Wigner's approximation [46] and is included in the rate constant because the transition state involves transfer of a H atom. The partition function $q^{\ddagger}_{CH_2O\cdot S}$ is for the transition state leading to the formation of formaldehyde.

Values for $\Delta E^{\ddagger}_{app}$ and k_{app} at 550 K are calculated for each of the active sites and are shown in Table 3. The value of $\Delta E^{\ddagger}_{app}$ decreases more significantly for sites with an O-vacancy than for sites without an O-vacancy as the number of V—O—Ti support bonds increases, as can be seen in Fig. 8. For example, $\Delta E^{\ddagger}_{app}$ decreases by 1.1 kcal/mol progressing from species **0** to **3**, whereas the decrease is >7 kcal/mol progressing from species **1d** to **3d**. The experimental values of $\Delta E^{\ddagger}_{app}$ for VO_x/SiO_2 [7] and VO_x/TiO_2 [8] are also shown and are in good agreement with the range of values on $\Delta E^{\ddagger}_{app}$ for sites on $VO_x/TiO_x/SiO_2$ containing an O-vacancy. The value of k_{app} changes by less than 20% as the number of V—O—Ti support bonds increases from zero to three for sites without an O-vacancy; however, the value of k_{app} increases by over a factor of 60 for sites with an O-vacancy, as shown in Fig. 9. Thus, the number of V—O—Ti support bonds strongly influences the activity of methanol oxidation for sites containing an O-vacancy.

An alternative pathway for methanol oxidation is the adsorption of methanol onto an active site containing a surface Ti—OH group, thereby forming a HO—V=O and H_3CO—Ti—OH species. One of the three methoxy H atoms is then abstracted by the vanadyl O to form a HO—V—OH and H_2CO—Ti—OH species. The weakly bound formaldehyde species rapidly desorbs, and water is released, reforming a V—O—Ti support bond. For this pathway, the change in energy for methanol adsorption is ΔE_{ads} = −8.6 kcal/mol and the activation energy for H-abstraction is $\Delta E^{\ddagger}_{rls}$ = 34.1 kcal/mol.

Table 3
Values for ΔE_{ads}, $\Delta E^{\ddagger}_{rls}$, $\Delta E^{\ddagger}_{app}$, and k_{app} for each of the active sites in Fig. 7. The top half of the table is for sites without an O-vacancy and the bottom half is for sites with an O-vacancy (denoted as *d*). Also shown are the values for VO_x on TiO_2. The support bond that is broken during methanol adsorption is indicated in parentheses. All energies are listed in kcal/mol. The value of k_{app} is reported for 550 K in units of $atm^{-1}\ s^{-1}$.

Active site	ΔE_{ads}	$\Delta E^{\ddagger}_{rls}$	$\Delta E^{\ddagger}_{app}$	k_{app} ($atm^{-1}\ s^{-1}$)
0, SiO_2[a]	−15.5 (V—O—Si)	39.8	24.3	8.93×10^{-3}
1	−15.0 (V—O—Si)	39.1	24.1	9.52×10^{-3}
2	−15.7 (V—O—Si)	39.0	23.3	9.80×10^{-3}
3	−15.4 (V—O—Ti)	38.6	23.2	1.07×10^{-2}
TiO_2[b]	−15.7 (V—O—Ti)	38.5	22.8	1.17×10^{-2}
1d	−15.4 (V—O—Ti)	38.6	23.2	2.40×10^{-2}
2d	−15.6 (V—O—Ti)	35.7	20.1	6.81×10^{-1}
3d	−15.4 (V—O—Ti)	34.3	18.9	1.35
TiO_2-d[b]	−15.9 (V—O—Ti)	31.8	15.9	1.48

[a] Ref. [27].
[b] Ref. [10].

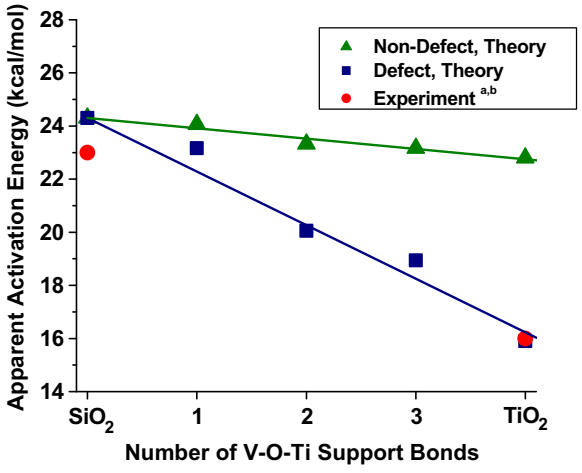

Fig. 8. Values of $\Delta E^{\ddagger}_{app}$ for active sites with a different number of V—O—Ti bonds ([a]Ref. [7] SiO_2. [b]Ref. [8] TiO_2).

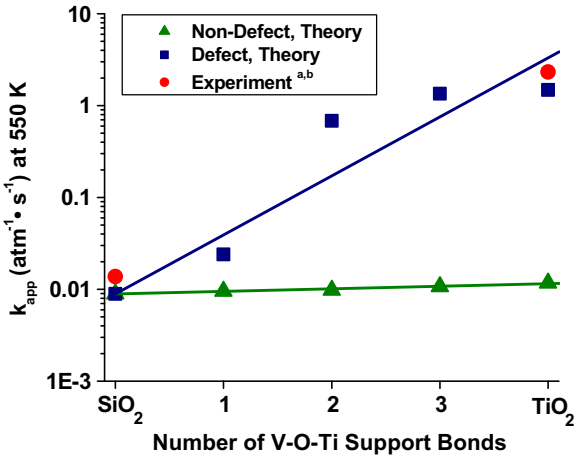

Fig. 9. Values of k_{app} for active sites with a different number of V—O—Ti bonds ([a]Ref. [7] SiO_2. [b]Ref. [8] TiO_2).

Using Eqs. (2)–(4), the value of k_{app} at 550 K for this pathway is 1.00×10^{-5} atm^{-1} s^{-1}, which is two orders of magnitude smaller than the value of k_{app} on non-defect sites, as shown in Table 3, and therefore, this reaction pathway was not considered further.

4.5. Model for the distribution of active sites

To compare the theoretical calculations with the experimental results, it is necessary to define the distribution of active sites on the surface. This was done by determining the distribution of Ti on SiO_2 and then V on TiO_x/SiO_2. Experimental work by Scott and coworkers [47] has shown that Ti grafts preferentially as Ti—O—Ti dimers ($[(\equiv SiO)Ti(O^iPr)_3]_2O$) onto a silica support when $Ti(O^iPr)_4$ is used as the Ti precursor, the same precursor used in the present study. This work suggests that upon calcination, Ti may exist primarily as $O_xTi—O—TiO_x$ species on the MCM-48 support. Correspondingly, V was assumed to have a low probability of bonding to only one Ti.

The distribution of V on the TiO_x/SiO_2 surface was determined in a manner similar to that for Ti. In this analysis, it was assumed that the V atoms are mobile on the surface during calcination but that the Si and Ti atoms are immobile. Calculations were performed to determine whether an energetic preference exists for V to graft to certain sites on the surface. From these calculations, V was found to prefer sites with three similar bonds, with V coordinated to 3 V—O—Ti support bonds favored by 2.03 kcal/mol relative to V coordinated to 3 V—O—Si support bonds. Active sites with 1 or 2 V—O—Ti support bonds were found not to be preferred energetically to sites with zero or 3 V—O—Ti support bonds because of the increased strain imparted to the cluster model by the difference in size between Ti and Si atoms. The trend in the relative energetic stability was used to determine the statistical distribution of these sites.

The preferential anchoring of VO_x species at TiO_x sites supported on SiO_2 deduced from the above analysis is supported by recent work by Lee and Wachs [14] on multilayered metal oxide supports, which shows that transition metals coordinate preferentially to surface metal oxide modifiers deposited on SiO_2. This observation further supports our previous assumption that there are a negligible number of active sites that contain 1 V—O—Ti support bond (species **1** and **1d**).

The fraction of V sites that contain x Ti support bonds, $P(x\,\mathrm{Ti}|\mathrm{V})$, can be determined using Bayes' probability theorem [48]. Briefly, $P(x\,\mathrm{Ti}|\mathrm{V})$ depends on the distribution of Ti and V atoms on the surface and the V surface coverage for isolated, non-interacting V sites. The overall distribution of active sites is explained in further detail in the Supplementary material. The distribution of sites with 0, 2, and 3 V—O—Ti support bonds ($P(0\,\mathrm{Ti}|\mathrm{V})$, $P(2\,\mathrm{Ti}|\mathrm{V})$, and $P(3\,\mathrm{Ti}|\mathrm{V})$, respectively) are plotted versus Ti surface coverage up to one monolayer (4 Ti/nm^2) in Fig. 10. As can be seen, the fraction of sites with 3 V—O—Ti support bonds increases greatly at low Ti surface coverage, consistent with the large increase in activity observed experimentally.

4.6. Surface O-vacancy concentration

We have used a thermodynamic model to determine the distribution of active sites that contain an O-vacancy, consistent with previous work on VO_x/TiO_2 [10]. An equilibrium was assumed to exist between active sites with an O-vacancy, represented as $[V-D]_x$, and an active site without an O-vacancy, represented as $[V-O]_x$. A $[V-D]_x$ site can be formed from a $[V-O]_x$ site by migration of an O-vacancy contained between either a Ti—Ti or Ti—Si surface bond, as shown in Eq. (5), where D and O stand for the presence and absence of an O-vacancy, respectively.

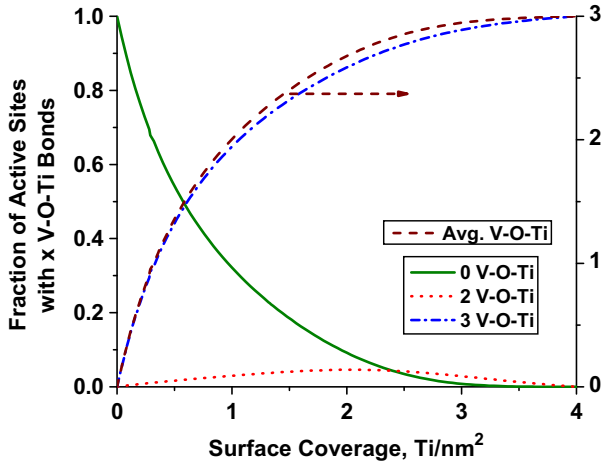

Fig. 10. The fraction of active sites with 0, 2, and 3 V—O—Ti support bonds (left axis) and the average number of V—O—Ti support bonds per active site (right axis) plotted versus Ti surface coverage.

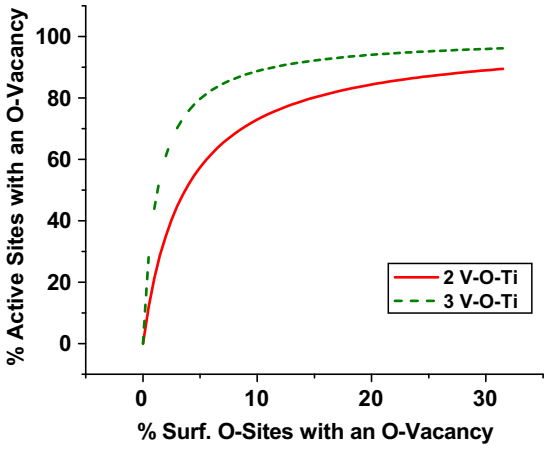

Fig. 11. Percent of active sites with an O-vacancy versus the total surface O-vacancies at 550 K. The curves are for active sites containing 2 or 3 V—O—Ti support bonds. Active sites containing 0 V—O—Ti (3 V—O—Si) support bonds have been assumed to have no O-vacancies. The plot for the case of 2.8 Ti/nm^2 is shown.

$$[V-O]+[D] \overset{K_{def}}{\rightleftarrows} [V-D]+[O] \quad (5)$$

Separate equilibrium constants were determined for the exchange of an O-vacancy in a Ti—Ti bond ($K_{def,x,Ti}$) or a Ti—Si bond ($K_{def,x,Si}$) with an O atom near an isolated vanadate species containing x V—O—Ti support bonds at 550 K. The value of these equilibrium constants are comparable for species with the same number of V—O—Ti support bonds, although there is a slight preference for the exchange of an O-vacancy in a Ti—Ti bond compared to that in a Ti—Si bond.

These calculations show that O-vacancies present on the surface of $VO_x/TiO_x/SiO_2$ prefer to be near vanadate species, since all values of $K_{def,x,Ti}$ and $K_{def,x,Si}$ are greater than one, especially for active sites with 3 V—O—Ti support bonds. This conclusion is in good agreement with the distribution of surface O-vacancies calculated for VO_x/TiO_2 [10]. The relationship between the fraction of vanadate species with x V—O—Ti support bonds containing an adjacent O-vacancy, $\frac{[V-D]_x}{[V-D]_x+[V-O]_x}$, and the fraction of possible surface O-vacancies per Ti atom, $\frac{[D]}{[Ti]}$, are plotted in Fig. 11. The determination of $K_{def,x,Ti}$ and $K_{def,x,Si}$, and the system of equations solved to generate Fig. 11 are discussed further in the Supplementary material.

4.7. Overall kinetics

The apparent first-order rate constant (k_{app}) at 550 K and the apparent activation energy ($\Delta E^{\ddagger}_{app}$) can be calculated using the distribution of active sites discussed previously, either with or without an O-vacancy. The value for k_{app} was determined by considering the contribution of each active site to the total rate constant, as shown in Eq. (6). Since it was previously assumed that Ti grafts to the SiO_2 surface as Ti dimers, consistent with prior experimental work [47], the sum in Eq. (6) is over all sites with 0, 2, or 3 V—O—Ti support bonds with and without an O-vacancy. This includes sites **0**, **2**, **2d**, **3**, and **3d** in Fig. 7 and omits sites **1** and **1d**, which only contain 1 V—O—Ti support bond.

$$k_{app} = \sum_{x=0,2,3} \{k_{app,x,O}\theta_{x,O} + k_{app,x,D}\theta_{x,D}\} \quad (6)$$

The values for $k_{app,x,O}$ and $k_{app,x,D}$, where x equals the number of V—O—Ti support bonds, are shown in Table 3. The fraction of each active site can be determined from the distribution shown in Fig. 10 and the concentration of surface O-vacancies shown in Fig. 11. It is noted further that not all O-vacancies are oxidized on the catalyst surface during methanol oxidation, despite the presence of O_2 [10,49]. The value of k_{app} at 550 K is plotted in Fig. 12 as a function of Ti surface coverage for assumed percentages of surface O-vacancies of 1%, 2%, and 5%. The theoretical results correctly capture the dramatic increase in activity measured experimentally. For a constant vanadia surface coverage, the TOF, and hence the value of k_{app}, increases systematically with Ti loading, as previously indicated by Wachs and coworkers [12]. Fig. 12 shows that sites containing an O-vacancy (species **2d** and **3d**) contribute to over 80% of the total observed rate.

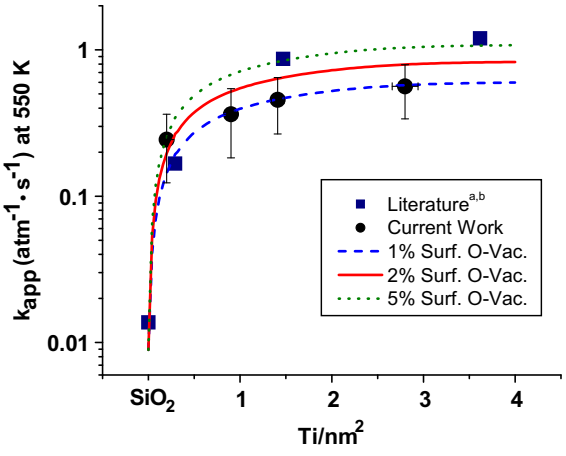

Fig. 12. The apparent first-order rate constant at 550 K for methanol oxidation plotted versus the surface coverage of Ti. The surface was assumed to consist only of active sites with 0 (species **0**) 2 (species **2**, **2d**), and 3 (species **3**, **3d**) V—O—Ti support bonds. The curves calculated from theoretical calculations are shown assuming 1%, 2%, and 5% surface O-vacancies ([a]Ref. [7]. [b]Ref. [39] (0.29, 1.47, 3.617 Ti/nm^2)).

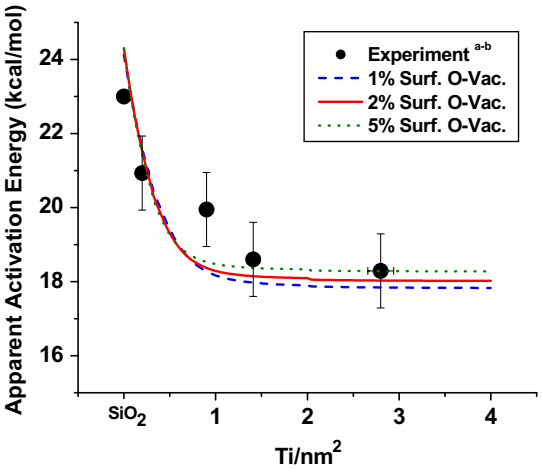

Fig. 13. The apparent activation energy for methanol oxidation plotted versus the surface coverage of Ti. The surface was assumed to consist only of active sites with 0 (species **0**), 2 (species **2**, **2d**), and 3 (species **3**, **3d**) V—O—Ti support bonds. The curves calculated from theoretical calculations are shown assuming 1%, 2%, and 5% surface O-vacancies ([a]Ref. [7] (SiO_2). [b]Present work (0.2, 0.9, 1.4, 2.8 Ti/nm^2)).

Similar agreement between theoretical and experimental work is also seen in a plot of $\Delta E^{\ddagger}_{app}$ versus Ti surface coverage, as shown in Fig. 13. The theoretical results indicate that there is a sharp decline in $\Delta E^{\ddagger}_{app}$, as confirmed by the experimental work in the present study. It should be noted that for Ti surface coverages below 0.5 Ti/nm^2, $\Delta E^{\ddagger}_{app}$ is lower when there is a higher fraction of surface O-vacancies; however, this trend reverses above 0.5 Ti/nm^2, in which case $\Delta E^{\ddagger}_{app}$ is lower when there is a lower fraction of surface O-vacancies. This trend is unexpected because having more active sites with an O-vacancy (species **2d** and **3d**) increases the apparent rate constant, as seen in Fig. 12, and should lower $\Delta E^{\ddagger}_{app}$. However, the activation energy becomes more sensitive to Ti surface coverage as the fraction of O-vacancies decreases, and as a consequence the ordering of the 1% and 5% curves in Fig. 13 reverses.

5. Conclusions

$VO_x/TiO_2/SiO_2$ catalysts have been synthesized with a constant V surface coverage of 0.7 V/nm^2 and Ti surface coverages ranging from 0.2 to 2.8 Ti/nm^2. The Ti atoms are bonded directly to the support through Ti—O—Si bonds, and V atoms are present as isolated vanadate species bonded to the support through a combination of V—O—Si and V—O—Ti bonds. For a fixed surface density of V atoms, the activity of $VO_x/TiO_2/SiO_2$ catalysts for methanol oxidation increases rapidly with increasing surface density of Ti, and the apparent activation energy decreases from 23 kcal/mol for 0.3 VO_x/SiO_2 to 18 kcal/mol for 0.7 $VO_x/2.8TiO_2/SiO_2$. The active site on $VO_x/TiO_2/SiO_2$ is well represented by a cluster model. The introduction of an oxygen vacancy between two Ti atoms adjacent to the active site decreases the apparent activation energy and

increases the apparent rate coefficient for the oxidation of methanol. The experimentally observed variation in the apparent rate coefficient and the apparent activation energy with Ti surface coverage are well described by a theoretical model that takes into account the distribution to Ti atoms on the surface of silica, the fraction of active sites with 0, 2, and 3 V—O—Ti support bonds, and the rate parameters determined for each of these active sites.

Acknowledgments

This work was supported by the Director, Office of Energy Research, Office of Basic Energy Sciences, Chemical Science Division, of the US Department of Energy under Contract No. DE-AC02-05CH11231 and by the Methane Conversion Cooperative funded by BP. Portions of this research were carried out at the Stanford Synchrotron Radiation Lightsource, a national user facility operated by Stanford University on behalf of the US Department of Energy, Office of Basic Energy Sciences. The SSRL Structural Molecular Biology Program is supported by the Department of Energy, Office of Biological and Environmental Research, and by the National Institutes of Health, National Center for Research Resources, Biomedical Technology Program.

Appendix A. Supplementary material

Supplementary data associated with this article can be found, in the online version, at doi:10.1016/j.jcat.2009.12.017.

References

[1] G. Deo, I.E. Wachs, J. Catal. 146 (1994) 323–334.
[2] L.J. Burcham, I.E. Wachs, Catal. Today 49 (1999) 467–484.
[3] S.Y. Lim, G.L. Haller, Appl. Catal. A 188 (1999) 277–286.
[4] M. Baltes, K. Cassiers, P. Van Der Voort, B.M. Weckhuysen, R.A. Schoonheydt, E.F. Vansant, J. Catal. 197 (2001) 160–171.
[5] L.J. Burcham, M. Badlani, I.E. Wachs, J. Catal. 203 (2001) 104–121.
[6] L.J. Burcham, L.E. Briand, I.E. Wachs, Langmuir 17 (2001) 6164–6174.
[7] J.L. Bronkema, A.T. Bell, J. Phys. Chem. C 111 (2007) 420–430.
[8] J.L. Bronkema, D.C. Leo, A.T. Bell, J. Phys. Chem. C 111 (2007) 14530–14540.
[9] I.E. Wachs, Catal. Today 100 (2005) 79–94.
[10] A. Goodrow, A.T. Bell, J. Phys. Chem. C 112 (2008) 13204–13214.
[11] J.M. Jehng, I.E. Wachs, Catal. Lett. 13 (1992) 9–19.
[12] X.T. Gao, S.R. Bare, J.L.G. Fierro, I.E. Wachs, J. Phys. Chem. B 103 (1999) 618–629.
[13] E.L. Lee, I.E. Wachs, J. Catal. 258 (2008) 103–110.
[14] E.L. Lee, I.E. Wachs, J. Phys. Chem. C 112 (2008) 20418–20428.
[15] K.L. Fujdala, T.D. Tilley, J. Am. Chem. Soc. 123 (2001) 10133–10134.
[16] S.D. Kelly, D. Hesterberg, B. Ravel, in: A.L. Ulery, L.R. Drees, (Eds.), Methods of Soil Analysis. Soil Science Society of America, Madison, WI, 2008.
[17] R.E. Jentoft, S.E. Deutsch, B.C. Gates, Rev. Sci. Instrum. 67 (1996) 2111–2112.
[18] M. Newville, J. Synchrotron Radiat. 8 (2001) 96–100.
[19] B. Ravel, M. Newville, J. Synchrotron Radiat. 12 (2005) 537–541.
[20] Y. Shao, L.F. Molnar, Y. Jung, J. Kussmann, C. Ochsenfeld, S.T. Brown, A.T.B. Gilbert, L.V. Slipchenko, S.V. Levchenko, D.P. O'Neill, R.A. DiStasio, R.C. Lochan, T. Wang, G.J.O. Beran, N.A. Besley, J.M. Herbert, C.Y. Lin, T. Van Voorhis, S.H. Chien, A. Sodt, R.P. Steele, V.A. Rassolov, P.E. Maslen, P.P. Korambath, R.D. Adamson, B. Austin, J. Baker, E.F.C. Byrd, H. Dachsel, R.J. Doerksen, A. Dreuw, B.D. Dunietz, A.D. Dutoi, T.R. Furlani, S.R. Gwaltney, A. Heyden, S. Hirata, C.P. Hsu, G. Kedziora, R.Z. Khalliulin, P. Klunzinger, A.M. Lee, M.S. Lee, W. Liang, I. Lotan, N. Nair, B. Peters, E.I. Proynov, P.A. Pieniazek, Y.M. Rhee, J. Ritchie, E. Rosta, C.D. Sherrill, A.C. Simmonett, J.E. Subotnik, H.L. Woodcock, W. Zhang, A.T. Bell, A.K. Chakraborty, D.M. Chipman, F.J. Keil, A. Warshel, W.J. Hehre, H.F. Schaefer, J. Kong, A.I. Krylov, P.M.W. Gill, M. Head-Gordon, Phys. Chem. Chem. Phys. 8 (2006) 3172–3191.
[21] A.P. Scott, L. Radom, J. Phys. Chem. 100 (1996) 16502–16513.
[22] B. Peters, A. Heyden, A.T. Bell, A. Chakraborty, J. Chem. Phys. 120 (2004) 7877–7886.
[23] A. Goodrow, A.T. Bell, M. Head-Gordon, J. Chem. Phys. 129 (2008) 174109.
[24] L. Noodleman, J. Chem. Phys. 74 (1981) 5737–5743.
[25] R. Caballol, O. Castell, F. Illas, P.R. Moreira, J.P. Malrieu, J. Phys. Chem. A 101 (1997) 7860–7866.
[26] J. Döbler, M. Pritzsche, J. Sauer, J. Am. Chem. Soc. 127 (2005) 10861–10868.
[27] A. Goodrow, A.T. Bell, J. Phys. Chem. C 111 (2007) 14753–14761.
[28] C. Zener, Proc. R. Soc. Lond. A 137 (1932) 696–702.
[29] C. Zener, Proc. R. Soc. Lond. A 140 (1933) 660–668.
[30] J.I. Steinfeld, J.S. Francisco, W.L. Hase, Chemical Kinetics & Dynamics, second ed., Prentice Hall, Upper Saddle River, 1999.
[31] A. Heyden, B. Peters, A.T. Bell, F.J. Keil, J. Phys. Chem. B 109 (2005) 1857–1873.
[32] D. Chandler, Introduction to Modern Statistical Mechanics, Oxford University Press, New York, NY, 1987.
[33] D.A. McQuarrie, Statistical Mechanics, University Science Books, Sausalito, CA, 2000.
[34] M.S. Morey, A. Davidson, G.D. Stucky, J. Porous Mater. 5 (1998) 195–204.
[35] P. Van der Voort, M. Mathieu, F. Mees, E.F. Vansant, J. Phys. Chem. B 102 (1998) 8847–8851.
[36] B.A. Morrow, Spectroscopic Characterization of Heterogeneous Catalysts, Elsevier, New York, NY, 1990.
[37] X.T. Gao, S.R. Bare, J.L.G. Fierro, M.A. Banares, I.E. Wachs, J. Phys. Chem. B 102 (1998) 5653–5666.
[38] X.T. Gao, I.E. Wachs, Catal. Today 51 (1999) 233–254.
[39] X. Gao, S.R. Bare, J.L.G. Fierro, I.E. Wachs, J. Phys. Chem. B 103 (1999) 618–629.
[40] X.T. Gao, S.R. Bare, B.M. Weckhuysen, I.E. Wachs, J. Phys. Chem. B 102 (1998) 10842–10852.
[41] F.D. Hardcastle, I.E. Wachs, J. Phys. Chem. 95 (1991) 5031–5041.
[42] F. Farges, G.E. Brown, J.J. Rehr, Phys. Rev. B 56 (1997) 1809–1819.
[43] J.M. Notestein, L.R. Andrini, V.I. Kalchenko, F.G. Requejo, A. Katz, E. Iglesia, J. Am. Chem. Soc. 129 (2007) 1122–1131.
[44] G. Pacchioni, Solid State Sci. 2 (2000) 161–179.
[45] M.V. Ganduglia-Pirovano, A. Hofmann, J. Sauer, Surf. Sci. Rep. 62 (2007) 219–270.
[46] R.I. Masel, Chemical Kinetics & Catalysis, Wiley, Interscience, New York, NY, 2001.
[47] A.O. Bouh, G.L. Rice, S.L. Scott, J. Am. Chem. Soc. 121 (1999) 7201–7210.
[48] A. Papoulis, Probability, Random Variables, and Stochastic Processes, McGraw-Hill, New York, 1984.
[49] S. Wendt, P.T. Sprunger, E. Lira, G.K.H. Madsen, Z.S. Li, J.O. Hansen, J. Matthiesen, A. Blekinge-Rasmussen, E. Laegsgaard, B. Hammer, F. Besenbacher, Science 320 (2008) 1755–1759.